Temperature Dependent Stress–Strain Behavior and Martensite Stabilization in Magnetic Shape Memory Ni$_{51.1}$Fe$_{16.4}$Ga$_{26.3}$Co$_{6.2}$ Single Crystal

Patricia Lázpita [1,*], Elena Villa [2], Francesca Villa [2] and Volodymyr Chernenko [1,3]

[1] Basque Center for Materials Applications and Nanostructures, University of Basque Country (UPV/EHU), Parque Científico UPV/EHU, 48940 Leioa, Spain; volodymyr.chernenko@ehu.eus
[2] CNR ICMATE Sede di Lecco, Via Previati n.1/e, 23900 Lecco, Italy; elena.villa@cnr.it (E.V.); francesca.villa@icmate.cnr.it (F.V.)
[3] Ikerbasque, Basque Foundation for Science, 48009 Bilbao, Spain
* Correspondence: patricia.lazpita@ehu.eus; Tel.: +34-94-601-5086

Abstract: The superelastic properties and stress-induced martensite (SIM) stabilization have been studied in a shape memory Ni$_{51.1}$Fe$_{16.4}$Ga$_{26.3}$Co$_{6.2}$ single crystal. The single crystal, characterized by a thermally induced forward martensitic transformation temperature around 56 °C in the initial state, has been submitted to compression mechanical testing at different temperatures well above, near and below the martensitic transformation (MT). After each mechanical test, the characteristic MT temperatures and the transformation enthalpy have been monitored by means of differential scanning calorimetry. At temperatures below MT, the stress–strain (σ–ε) curves show a large strain, around 6.0%, resulting from the detwinning process in the martensitic microstructure, which remains accumulated after unloading in the detwinned state of the sample as a typical behavior of the shape memory alloys (SMAs). After just two "σ–ε + heating" cycles the accumulation of strain was not observed any more indicating the formation of a two-way shape memory effect which consists in a spontaneous recovery of the aforementioned detwinned state of the sample during its cooling across the forward MT. Whereas the thermally induced shape recovery in conventional SMAs occurs at the fixed value of the reverse MT temperature, the heating DSC curves of the mechanically deformed martensite in the present work show a burst-like calorimetric peak at the reverse MT arising at temperatures essentially higher than the thermally activated one. This behavior is the result of the SIM stabilization effect. After a short thermal aging in the stress-free state, this effect almost disappears, showing a slight impact on the MT characteristic temperatures and the enthalpy. At temperatures higher than the transformation one, the SIM is not stabilized, as the mechanically induced martensite fully retransforms into austenite after the unloading. From the σ–ε curves, the critical stress, σ$_c$, as well as the values of Young's moduli of martensite and austenite are determined showing linear dependences on the temperature with a slope of 3.6 MPa/°C.

Keywords: martensitic transformation; superelastic effect; stress-induced stabilization of martensite; critical stress; Young's modulus

1. Introduction

Ferromagnetic shape memory alloys (FSMAs) have become a subject of great interest for high technology applications due to the giant strains, up to 12%, that they can exhibit in response to the external mechanical stress or magnetic field [1–3]. The strong magnetoelastic coupling in these compounds allows controlling the large deformation in a reversible way by the applied magnetic field, thereby opening new possibilities in the development of actuators and sensors [4]. In addition to the shape memory effect (SME) and the superelastic effect (SE) showed by the conventional shape memory compounds, the FSMAs exhibit the so-called magnetic field-induced strain (MFIS). The main mechanism that governs this

effect is the reorientation of martensitic variants, which requires an appreciable value of the equivalent magnetostress larger than the twinning stress [5]. Obviously, the stabilization of martensite can increase the twinning stress, thereby impeding a large MFIS.

Martensite stabilization can be achieved by thermal, chemical, mechanical or thermomechanical treatment (see, e.g., [6,7] and references therein). The different degrees of the martensite stabilization were obtained by heat treatment, e.g., in polycrystalline $Ni_{54}Fe_{16}Ga_{27}Mn_3$ and $Ni_{52}Fe_{18}Ga_{27}Co_3$ FSMAs, explained by a quenched-in disorder [8], or by aging of the stress-induced martensite (SIM-aging) in a single crystalline $Co_{49}Ni_{21}Ga_{30}$, explained within the concept of symmetry-conforming short-range order [9]. Recently, SIM-aging effects on the acoustic emission and the entropy accompanying MT were studied in the $Ni_{51}Fe_{18}Ga_{27}Co_4$ single crystal [10]. It is worth noting that in almost all aforementioned FSMAs the γ'-precipitates were present contributing, to some extent, to a martensite stabilization [8,9].

Stabilization of martensitic phase can also occur after its mechanical deformation resulting in the detwinned state of martensite, in this case it is called a stress-induced martensite stabilization (SIM stabilization). The fact of SIM stabilization, which is basically related to the formation of the non-equilibrium microstructure of martensitic phase, can be revealed by the enhanced temperature of the thermally induced reverse MT, whereas the forward MT remains intact. The difficulties in forming a habit plane between the austenite and the detwinned martensite were considered to be an origin of this mechanical stabilization effect [11,12].

The external mechanical stress can be replaced by the internal one that can also promote the nucleation and growth of the twin variants in a preferential direction [13]. The internal stress can be created through the formation of dislocations and other defects in the lattice, coherent particles, but also the SIM can promote internal stresses that induce a growth of the oriented variants. The formation of the SIM-induced effects, such as a two-way SME or rubber-like behavior of martensite, has been investigated in single crystals of CoNiGa, CoNiAl, NiMnGa and NiFeGaCo FSMAs [9,14–21] showing a strong dependency of the growth and stabilization of the martensitic variants on temperature, stress and crystallographic orientation. Therefore, the elucidation of the conditions responsible for the SIM stabilization in FSMAs is highly desirable since this stabilization directly impacts their functionalities that they exhibit as the magnetically activated materials or as conventional SMAs [9,10].

Among Heusler type FSMAs, the NiFeGaCo alloys represent (to date) the only known analog to classical NiMnGa in terms of a giant MFIS that they show [3,22]. Compared to NiMnGa, these materials are much more ductile (see [23] and references therein) whereby they are much more sustainable to SE cycling, which is an important advantage for their applications in elastocaloric devices [24–26]. These materials are also interesting for their magnetocaloric [27] and magnetoresistance properties [28].

In the present study, we examine the superelastic properties and the stress-induced martensite stabilization in a single crystal of NiFeGaCo FSMA with composition which is not prone to showing a second-phase precipitation [29,30]. The stress–strain measurements have been systematically performed on the sample cut along $<110>_A$ crystallographic axis of the cubic austenite since the deformation in this direction is crucial for obtaining a giant rubber-like behavior in an SIM-aged conditioned martensitic state [19], or developing a two-way SME [14], or modifying a character of the thermally induced strain recovery in such FSMAs [31]. Thus, we carried out the compression mechanical tests along the $<110>_A$ direction at different temperatures: well above, near and below the martensitic transformation, whereby assessing the temperature range of the SIM stabilization and the impact of the mechanical stress on the character of MT.

2. Materials and Methods

A single crystalline ingot with a composition of $Ni_{51.1}Fe_{16.4}Ga_{26.3}Co_{6.2}$ (at.%) was grown by a floating zone method, solution treated at 900 °C for 24 h and water quenched.

The $<110>_A$ crystallographic orientation in cubic austenitic phase of the single crystal was determined by the Laue back-reflection method and a sample with this orientation was cut using electro-discharge machine (EDM). The alloy composition was determined with an uncertainty of 0.5 at.% by energy dispersive X-ray spectrometry (EDXS) and characterized in the initial quenched state by a two-step reverse MT at heating and thermally induced MT temperature around 56 °C at cooling. The alloy composition and heat treatment ensured the formation of the non-modulated tetragonal 2M-martensitic phase [32,33]. The multi- or two-step character of the reverse MT was observed in the literature for different SMAs (see, e.g., [34,35]) and may be explained by the formation of the nonuniform microstructure of martensite resulting from quenching: presumably, the main body of the sample consists of a thermally stabilized one-twin variant co-existing with the rest multitwinned part of sample. Whereas the latter part transforms at a fixed reverse MT temperature, the former part exhibits a jerky-like MT at higher temperatures resulting in an extension of the entire interval of reverse MT.

A cylindrical sample of 3 mm diameter and about 4 mm height has been tested by compression along the crystallographic $<110>_A$ direction at different temperatures and by the differential scanning calorimetry (DSC). For the mechanical tests, we used a MTS 2/M mechanical testing machine in compression configuration with a load cell of 10 kN and a climatic chamber. In this configuration, we measured the σ–ε curves in a stress control mode up to 350 MPa with a loading/unloading rate of about 20 MPa/min at constant temperatures varying from room temperature to 130 °C. The compression conditions were selected to prevent a possible sample failure and to achieve better accuracy of the measurements. To perform each σ–ε experiment the sample was heated from the room temperature up to the temperature value of the following test. Before the test and after each σ–ε cycle, in order to determine the MT characteristics of the currently unloaded sample, we recorded its DSC heating and cooling curves with a TA Instruments Q100 Calorimeter, in the temperature range between 10 °C and 200 °C with a heating/cooling rate of 10 °C/min. As the free sample was always in a martensitic phase at room temperature, all DSC measurements were started by heating through the reverse MT until 200 °C, holding at this temperature for 10 min to allow the complete recovery of the sample deformation induced by the compression, and then cooling back to the room temperature.

The crystal structure has been checked by X-ray diffraction from the basement of the cylindrical sample with a plane of $\{110\}_A$ used for compression, by an X'pert Panalytical diffractometer at room temperature before the first mechanical test and after all the thermomechanical tests.

3. Results and Discussion

Figure 1 shows the compression stress–strain, σ–ε, curves along the $<110>_A$ direction of the single crystalline sample at selected temperatures below, in the interval and above the reverse MT temperature, $A_s = 69$ °C, which was determined in the initial state before the mechanical test (see Table 1). Each σ–ε curve was recorded after the thermal treatment of the free sample at 200 °C, so the latter was initially in the thermally induced martensitic phase ($T < A_s$), martensitic/austenite two-phase state ($A_s < T < A_f$) and in the austenitic phase ($T > A_f$). At temperatures below A_s, i.e., at 22 °C and 40 °C, the curves show a plateau corresponding to the irreversible twin variant reorientation process followed by the elastic deformation of the martensitic phase reaching maximum strain of 9% at 350 MPa at 22 °C. This induced strain is only partly recovered after the unloading resulting in a residual deformation of around 6% related to SIM stabilization. This strain value, resulting from the detwinning process in the martensitic microstructure, is in line with the obtained one in the $<110>_A$ compression tests of the martensitic phases in NiFeGaCo [19] and NiMnGa [36]. The curve at 60 °C, also obtained below A_s, does not show the strain accumulation, only indicates the presence of the quasi-elastic σ–ε loop almost identical to the one for the oriented martensite obtained at 40 °C test. This suggests a spontaneous recovery of the aforementioned detwinned state of the free sample during cooling through the forward MT.

Such behavior is obviously related to the two-way shape memory effect (TWSME) which was developed after the two "σ–ε + heating" cycles at 22 °C and 40 °C. TWSME implies a spontaneous macroscopic shape change in the sample induced by cooling/heating through MT, where the martensitic variants are oriented in a preferable direction under internal stresses produced by the defect structure formed via a thermomechanical training. Thus, we think, that namely TWSME is responsible for the absence of plateau at 60 °C. We assume that the previous two stages of the thermomechanical treatment were enough to "train" the sample whereby the same martensitic variant, memorized from the previous compression tests, is obtained after DSC cooling of the trained sample through the forward MT to the room temperature. Therefore, σ–ε test at 60 °C reveals an elastic behavior of the spontaneously oriented martensitic variant. TWSME was also observed for single crystalline NiMnGa [15,18], CoNiAl [14] and NiFeGaCo [21] FSMAs.
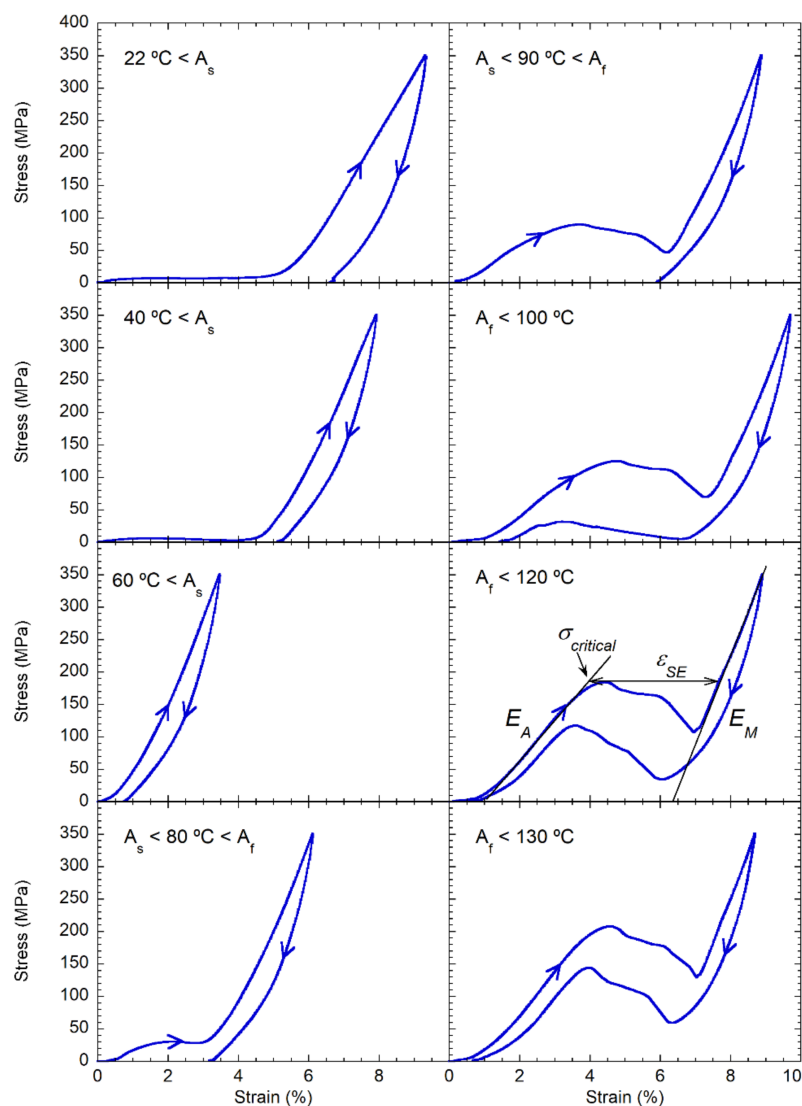
Figure 1. Stress–strain compression curves at different temperatures: below A_s = 69 °C, in the interval A_f-A_s, where A_f = 92 °C, and above A_f of the thermally induced reverse MT. The schematic at temperature 120 °C shows how the values of critical stress ($\sigma_{critical}$), superelastic strain (ε_{SE}), and Young's moduli of the austenitic (E_A) and martensitic (E_M) phases were determined.

Table 1. Characteristic parameters of the martensitic transformation before the compression tests and after the loading/unloading stress–strain (SS) cycles at different temperatures determined by means of the calorimetric measurements. The values of the forward martensitic transformation temperature start (M_s), finish (M_f) and enthalpy change ($\Delta H_{cooling}$) are obtained from the cooling ramps. Reverse martensitic transformation temperature start (A_s), finish (A_f) and the enthalpy change ($\Delta H_{heating}$) are extracted from the heating runs.

Temperature of SS Test Cycle		M_s (°C)	M_f (°C)	$\Delta H_{cooling}$ (J/g)	A_s (°C)	A_f (°C)	$\Delta H_{heating}$ (J/g)
$A_s < T$	before the tests	62	50	3.4	69	92	2.5
	after SS 22 °C	61	48	3.1	101	103	3.1
	after SS 40 °C	59	47	3.0	102	103	3.1
	after SS 60 °C	59	47	3.0	101	102	3.0
$A_s < T < A_f$	after SS 80 °C	59	46	3.0	99	100	3.1
	after SS 90 °C	58	46	3.1	98	100	3.1
$T > A_f$	after SS 100 °C	59	46	3.2	65	77	3.3
	after SS 120 °C	58	47	3.4	62	76	3.1
	after SS 130 °C	58	47	3.4	63	77	3.0

At temperatures in the interval A_f-A_s and above A_f, the stress-induced MT and a conventional superelastic behavior are observed. The initial slope at low applied stress corresponds to the elastic deformation of the austenitic phase, and at the critical stress values the induced first portion of the martensitic phase manifests itself as a plateau-like maximum on the curves followed by a decrease in the stress. Once the stress-induced MT is completed, the elastic deformation of the martensite is observed at high stresses.

At 80 °C and 90 °C, SE is incomplete due to the existence of thermal hysteresis of MT, so the unrecoverable residual strain remains after the unloading. This effect relates to the austenite/martensite mixture at these temperatures, hence only an austenite fraction is transforming.

At temperatures above A_f, the induced strain is perfectly superelastic reflecting a complete stress-induced MT from the austenitic phase to the martensitic one by loading that is fully reversible after unloading. In this case, there is no residual deformation after σ–ε cycle.

In all experiments in Figure 1, where the stress-induced MT is observed, the curves show a non-monotone stress–strain dependence just after achieving the critical stress necessary for the transformation. Such non-monotone σ–ε dependencies of the forward and reverse stress-induced MT indicate the non-equilibrium progression of the transformation between the austenitic and martensitic phases and is linked to the different stresses required for the nucleation and propagation of the interfaces between phases [37]. Actually, in [31] this compression behavior for the <110>$_A$ oriented NiFeGaCo single crystal was modeled in terms of the direct relationship between the elastic interface stresses and the MT kinetics. Similar tendencies have been also observed in the experiments on the NiMnGa, CoNiGa and CoNiAl single crystals [17,20,37,38] which show a non-monotonous behavior for applied stress in the <110> direction, as occurs in our specimen.

The elastic branches in the loading curves for the martensitic phase in Figure 1 show a rather linear behavior, whereas unloading branches demonstrate nonlinearity meaning that the sample expansion response does not follow the rate of stress removal. Therefore, the hysteretic behavior in this elastic branch is considered as the mostly instrumental one which may be attributed to the influence of frictional forces between the anvils and sample.

The data in Figure 1 have been used for the evaluation of the different parameters of the stress-induced MT according to the schematic depicted in the same figure at 120 °C. The total strain achieved in the superelastic region, ε_{SE}, was obtained as the difference between the strain in the austenitic phase and the martensitic one at the critical stress point (see schematic in Figure 1). One of the results is a moderate decrement of ε_{SE} with the temperature, from 4.2% at 100 °C to 3.6% at 130 °C, that may be associated with the growth of multiple variants due to improvement of the variant–variant interaction at higher

temperatures [39]. The stress hysteresis of the MT remains practically unchanged in the studied temperature range.

From stress–strain curves we have determined the phase diagram "critical stress versus temperature", $\sigma_{critical}$ (T), and the Young's moduli of the austenite (E_A) and martensite (E_M). The values of the critical stress or twinning stress at each temperature were defined by the two-tangent method, as the cross point of the linearly extrapolated slope related to the elasticity of either austenite or martensite and the extended straight line of the plateau region (see schematic in Figure 1). Figure 2a displays the twinning stress required for the variant reorientation in the martensitic phase at $T < A_s$ (open squares) and the critical stress of the stress-induced MT at $T > A_f$ (solid circles). It is seen that, while the twinning stress is slightly decreasing with the temperature, the critical stress for stress-induced MT linearly increases as a function of the temperature with a slope of 3.6 MPa/°C. This value is in line with those found in other Ni-Fe-Ga-based FSMAs [33,40]. It is easy to find that the extrapolated temperature value at zero stress, which gives the transformation temperature from the thermally induced martensite to the austenite, is in a good agreement with the DSC results (69 °C) (see Table 1). Figure 2b depicts temperature dependences of the Young's moduli of the austenite, E_A, and martensitic phase, E_M, evaluated from the slopes of the stress–strain curves corresponding to the quasilinear elastic deformation in the loading process. It has to be noted that E_M is much higher than E_A and presents two different dependencies on temperature, 100 MPa/°C for temperatures below MT, i.e., for the thermally induced martensite, and 34 MPa/°C at high temperatures for the stress-induced martensite. These tendencies are indicative of the different martensitic microstructures formed as a result of the free-sample cooling through MT (poly-variant martensitic phase) or as a result of the stress-induced MT (the sample consists of mainly one-variant of martensite). On the other hand, E_A presents a smooth increment with the temperature having a slope of 85 MPa/°C close in value to the temperature dependence of poly-variant state of martensite. The E_A(T) behavior agrees with the one observed in other FSMAs, such as, e.g., Co-Ni-Al or Ni-Mn-Ga, and has been explained by the decrement of the elastic constants due to the lattice softening when approaching the start of the forward MT [17,41].
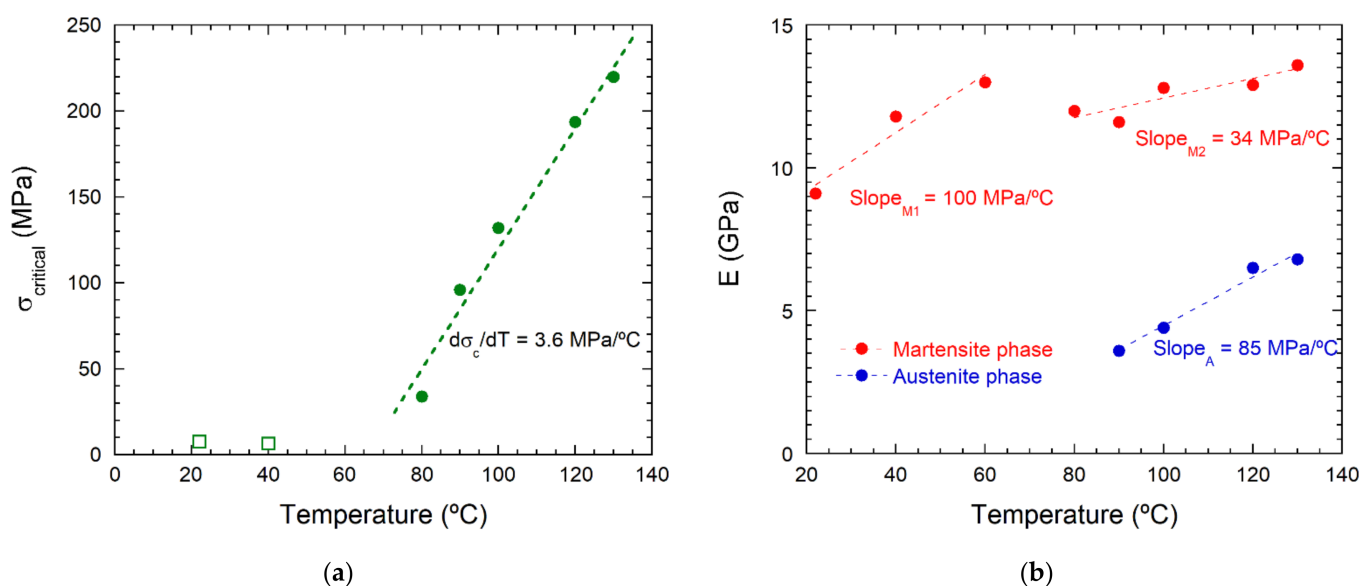
Figure 2. (**a**) Temperature dependence of the critical stress of the MT start (solid circles) and twinning stress (open squares). (**b**) Evolutions of Young's moduli, E_A and E_M, with the temperature. All lines are the linear fits to the data points.

To check the impact of the SIM on MT, after each mechanical test the characteristic MT temperatures of the sample and the enthalpy of the transformation (ΔH) have been monitored by means of differential scanning calorimetry. To this aim, the DSC curves

were recorded during heating the sample to 200 °C, holding for 10 min and subsequent cooling to the room temperature. The results of DSC measurements are shown in Figure 3 and Table 1. The anomalous shapes on DSC curves in Figure 3 vary strongly when one compares exothermic and some endothermic peaks. Whereas the former ones have a common cupola shape, the latter ones exhibit a burst-like behavior characterized by a very fast heat absorption causing a loop on the curve due to a short overcooling of the sample. In the case of such abnormal loops, the values of ΔH were determined by the integration of DSC signal over a time.
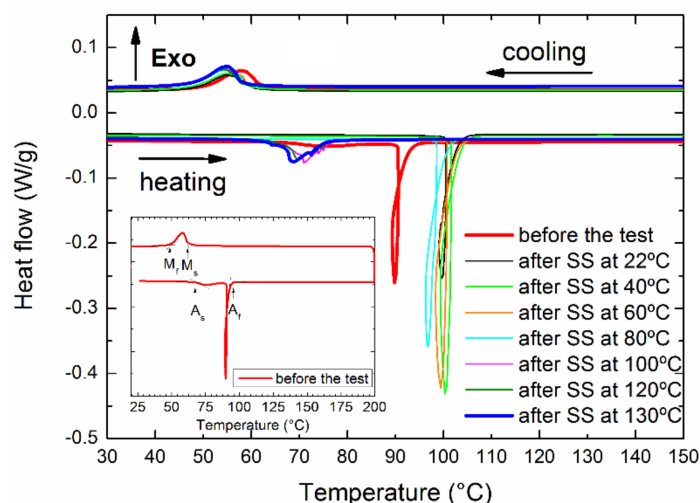
Figure 3. DSC heating and cooling runs measured before the first stress–strain (SS) test and after each compression SS cycle at the constant temperature indicated in the graphs. The inset illustrates the determination of the MT characteristic temperatures in the as-received sample before testing for which the two-step reverse MT is observed on the heating curve (see experimental section).

It is instructive to note that thermally activated forward MT during cooling gives rise to the overlapping single broad peaks. Thus, the different mechanical tests show a low impact on the forward MT only slightly affecting both the MT enthalpy, $\Delta H_{cooling} = (3.2 \pm 0.2)$ J/g, as the average value, and the MT start temperature, M_s, that varies in a range between 62 °C and 58 °C.

The DSC heating runs in Figure 3 reveal the different influence of the mechanical tests on the thermally activated reverse MT if they are compared with the cooling runs. The reverse MT manifests in DSC curves through two different behaviors. Firstly, after mechanical tests at temperatures lower than 100 °C ($A_f < 100$ °C), which involve a primary deformation of martensitic phase or its fraction, DSC heating runs show a sharp peak associated to the burst-like behavior in a range of temperatures between 98 °C and 102 °C shifting towards high temperatures, around 30 °C (Table 1), due to the effect of stress-induced stabilization of the martensite. Table 1 shows that the average values of $\Delta H_{heating}$ and $\Delta H_{cooling}$ are almost the same indicating the same amount of martensite involved in the thermally induced MT independently of mechanical tests. The reduced value of enthalpy for the reverse MT in the as-received sample, calculated using areas under two DSC peaks (Figure 3), could be due to an underestimation produced by the difficulty of area estimation for the very smeared first peak. After a short thermal aging of the stress-free sample at 200 °C, the DSC cooling runs exhibit peaks with characteristics corresponding to the initial state of the sample.

Secondly, after the mechanical tests at 100 °C and above, where the SE is complete, i.e., the strain is fully recovered due to the transformation into austenite, a broad DSC peak characterized by $A_s = 65$ °C (close to $A_s = 69$ °C of the diffuse peak for the as-received sample, Table 1) is observed, indicating no SIM stabilization effect. Therefore, it is clear that the stress-induced reorientation of the martensitic variants promotes the stabilization

of the martensitic phase to the higher temperatures by increasing A_s from (63–69) °C to (98–102) °C (Table 1). The difficulties in forming a habit plane between austenite and the twinned/ detwinned martensite, due to their lattice incompatibility, are considered to be an origin of the SIM stabilization effect (see, e.g., [11,12,35]).

Furthermore, X-ray diffraction patterns were measured with the intention to throw some light on the effect of the compression/temperature treatment on the growth of different martensitic variants. Diffractograms shown in Figure 4 were obtained at room temperature before the mechanical test, in the initial state of sample, and after all the "σ–ε + heating" cycles. The single crystal was oriented along the <110>$_A$ axis, so before the compression two reflections that correspond to the differently oriented martensitic variants are observed. These reflections fit with the non-modulated tetragonal unit cell with lattice parameters of a = 0.542 nm and c = 0.648 nm. This tetragonal unit cell is considered in the coordinates of the austenitic L2$_1$-ordered cubic lattice, whereby during MT it shrinks along two axes and expands along the third one. In this case, the value of c/a ratio is equal to about 1.2 which is a common value for FSMAs exhibiting a non-modulated tetragonal martensitic structure [19]. The cell parameters can be used to calculate the maximum possible SE strain which could be obtained due to a stress-induced MT. For that, the cell parameter of the cubic phase was accepted to be a_0 = 0.588 nm which was measured for Ni$_{51}$Fe$_{18}$Ga$_{27}$Co$_4$ [19,42]. Taking into account the above values of a, c and a_0, in compression tests along <110>$_A$ direction the maximum calculated strain is equal to about 6.0% which is by about 40% larger than the experimental strains ε_{SE} determined from the experimental data in Figure 1 by the method shown inside it at T = 120 °C. This difference is indicative of the multivariant martensitic state induced during compressions tests, which is even more relevant at higher temperatures.
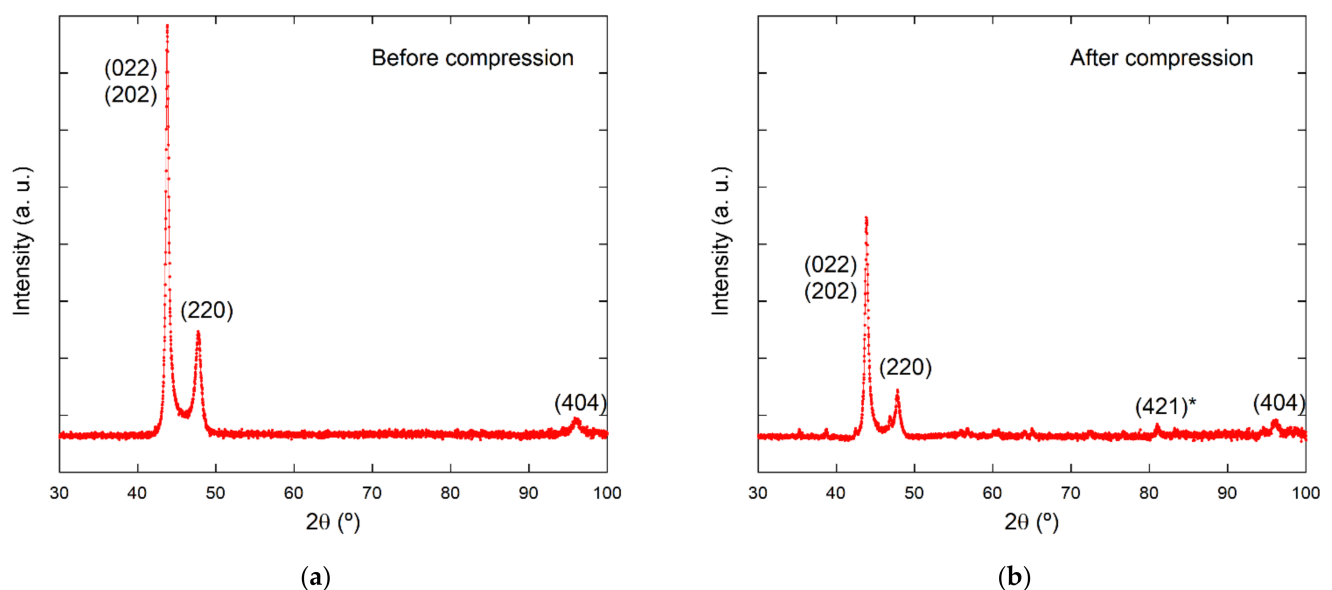
Figure 4. X-ray diffraction patterns of the basement surface of the sample in the martensitic state measured at room temperature: (**a**) before thermomechanical testing and (**b**) after the thermomechanical treatment.

It has to be noted that after compression in the <110>$_A$ direction, the main reflections remain at the same position, but their intensities are drastically reduced alongside the appearance of a new tiny peak indicated in Figure 4 by an asterisk. All these features in diffraction patterns could be related to the growth or disappearance of differently oriented martensitic variants. In order to determine the redistribution of the different martensitic variants, we estimate the relative change in the intensity between different reflections. To this aim we calculate the ratio between the integrated intensity of the (202)/(022) and (220) reflections before and after compression. Before the compression, there is a random variant

orientation of one-third for each direction, with the relation 1:1:1 for the reflections (022), (202) and (220), respectively. However, after the cycling there is a drastic intensity reduction, by half, of the intensity of the principal reflections, although they present practically the same distribution ratio of 1:1:1. This fact can be related to the growth of variants with other orientations that would be favored by residual internal stresses or defects generated during the thermomechanical treatment. Moreover, in the diffraction pattern there are no peaks corresponding to the austenite phase, which corroborates the complete reversibility of the stress-induced MT confirming the DSC results.

4. Summary

The stress–strain behavior and stress-induced martensite (SIM) stabilization have been studied in a shape memory $Ni_{51.1}Fe_{16.4}Ga_{26.3}Co_{6.2}$ (at.%) single crystal under compression along the $<110>_A$ direction at different temperatures: well above, near and below the reverse martensitic transformation. At temperatures below MT, the stress–strain curves show a large strain, around 6.0%, related to the detwinning process in the martensitic microstructure, which keeps accumulating after unloading due to the stabilized character of the mechanically deformed martensite. Calorimetric analysis shows a burst-like calorimetric peak at about 100 °C which corresponds to the reverse MT of mechanically deformed martensite. This value of the reverse MT start temperature is much higher than the thermally activated one (69 °C) obtained for the sample in its initial state, reflecting a martensitic phase stabilization. The difficulties in forming a habit plane between the austenite and the twinned/ detwinned martensite, due to their lattice incompatibility, are considered to be an origin of the SIM stabilization effect. At temperatures from 100 °C to 130 °C, the superelastic effect is entirely reversible. The superelastic strain was found to be reduced, if compared with the one calculated using the lattice parameters, due to the growth of multiple variants. In contrast to mechanically deformed martensite, SIM at high temperatures, induced from austenitic phase, is not stabilized due to a complete recovery after the stress unloading through reverse MT. The critical stress, σ_c, versus temperature phase diagram shows a linear increment when the temperature increases, with a slope $d\sigma_c/dT$ of 3.6 MPa/°C. Moreover, in this case the characteristic temperatures of the thermally induced MT remain practically constant after the stress cycling.

The present work demonstrates that the phenomenon of SIM stabilization should be taken into account in the case of the need for cyclic actuation using a single crystalline FSMA.

Author Contributions: Conceptualization, E.V. and V.C.; data curation, P.L., E.V. and F.V.; formal analysis, P.L., E.V. and F.V.; funding acquisition, E.V. and V.C.; investigation, P.L., E.V. and F.V.; methodology, E.V. and F.V.; resources, E.V. and F.V.; supervision, E.V. and V.C.; writing—original draft, P.L. and V.C.; writing—review and editing, P.L., E.V. and V.C. All authors have read and agreed to the published version of the manuscript.

Conflicts of Interest: The authors declare no conflict of interest.

References

1. Sozinov, A.; Lanska, N.; Soroka, A.; Zou, W. 12% magnetic field-induced strain in Ni-Mn-Ga-based non-modulated martensite. *Appl. Phys. Lett.* **2013**, *102*, 021902. [CrossRef]
2. Müllner, P.; Chernenko, V.A.; Kostorz, G. Large cyclic magnetic-field-induced deformation in orthorhombic (14M) Ni–Mn–Ga martensite. *J. Appl. Phys.* **2004**, *95*, 1531–1536. [CrossRef]
3. Morito, H.; Fujita, A.; Oikawa, K.; Ishida, K.; Fukamichi, K.; Kainuma, R. Stress-assisted magnetic-field-induced strain in Ni–Fe–Ga–Co ferromagnetic shape memory alloys. *Appl. Phys. Lett.* **2007**, *90*, 062505. [CrossRef]
4. Pagounis, E.; Muellner, P. Materials and Actuator Solutions for Advanced Magnetic Shape Memory Devices. In Proceedings of the ACTUATOR 2018, 16th International Conference on New Actuators, Bremen, Germany, 25–27 June 2018; pp. 1–7.

5. Heczko, O. Magnetic shape memory effect and highly mobile twin boundaries. *Mater. Sci. Technol. UK* **2014**, *30*, 1559–1578. [CrossRef]

6. Kustov, S.; Pons, J.; Cesari, E.; Van Humbeeck, J. Chemical and mechanical stabilization of martensite. *Acta Mater.* **2004**, *52*, 4547–4559. [CrossRef]

7. Oliveira, J.P.; Fernandes, F.M.B.; Schell, N.; Miranda, R.M. Martensite stabilization during superelastic cycling of laser welded NiTi plates. *Mater. Lett.* **2016**, *171*, 273–276. [CrossRef]

8. Picornell, C.; Pons, J.; Cesari, E.; Dutkiewicz, J. Thermal characteristics of Ni–Fe–Ga–Mn and Ni–Fe–Ga–Co ferromagnetic shape memory alloys. *Intermetallics* **2008**, *16*, 751–757. [CrossRef]

9. Niendorf, T.; Krooß, P.; Somsen, C.; Eggeler, G.; Chumlyakov, Y.I.; Maier, H.J. Martensite aging-Avenue to new high temperature shape memory alloys. *Acta Mater.* **2015**, *89*, 298–304. [CrossRef]

10. Samy, N.M.; Daróczi, L.; Tóth, L.Z.; Panchenko, E.; Chumlyakov, Y.; Surikov, N.; Beke, D.L. Effect of stress-induced martensite stabilization on acoustic emission characteristics and the entropy of martensitic transformation in shape memory $Ni_{51}Fe_{18}Ga_{27}Co_4$ single crystal. *Metals* **2020**, *10*, 534. [CrossRef]

11. Picornell, C.; Pons, J.; Cesari, E. Stabilisation of martensite by applying compressive stress in Cu-Al-Ni single crystals. *Acta Mater.* **2001**, *49*, 4221–4230. [CrossRef]

12. Roytburd, A.L. Intrinsic hysteresis of superelastic deformation. *Mater. Sci. Forum* **2000**, *327–328*, 389–392. [CrossRef]

13. Singh, S.; Kushwaha, P.; Scheibel, F.; Liermann, H.P.; Barman, S.R.; Acet, M.; Felser, C.; Pandey, D. Residual stress induced stabilization of martensite phase and its effect on the magnetostructural transition in Mn-rich Ni-Mn-In/Ga magnetic shape-memory alloys. *Phys. Rev. B-Condens. Matter Mater. Phys.* **2015**, *92*, 1–6. [CrossRef]

14. Panchenko, E.; Eftifeeva, A.; Chumlyakov, Y.; Gerstein, G.; Maier, H.J. Two-way shape memory effect and thermal cycling stability in $Co_{35}Ni_{35}Al_{30}$ single crystals by low-temperature martensite ageing. *Scr. Mater.* **2018**, *150*, 18–21. [CrossRef]

15. Timofeeva, E.E.; Panchenko, E.Y.; Pichkaleva, M.V.; Tagiltsev, A.I.; Chumlyakov, Y.I. The effect of stress-induced martensite ageing on the two-way shape memory effect in $Ni_{53}Mn_{25}Ga_{22}$ single crystals. *Mater. Lett.* **2018**, *228*, 490–492. [CrossRef]

16. Panchenko, E.; Chumlyakov, Y.; Maier, H.J.; Timofeeva, E.; Karaman, I. Tension/compression asymmetry of functional properties in [001]-oriented ferromagnetic NiFeGaCo single crystals. *Intermetallics* **2010**, *18*, 2458–2463. [CrossRef]

17. Li, P.; Karaca, H.E.; Chumlyakov, Y.I. Orientation dependent compression behavior of $Co_{35}Ni_{35}Al_{30}$ single crystals. *J. Alloys Compd.* **2017**, *718*, 326–334. [CrossRef]

18. Chernenko, V.A.; Villa, E.; Besseghini, S.; Barandiarán, J.M. Giant two-way shape memory effect in high-temperature Ni–Mn–Ga single crystal. *Phys. Procedia* **2010**, *10*, 94–98. [CrossRef]

19. Panchenko, E.; Timofeeva, E.; Eftifeeva, A.; Osipovich, K.; Surikov, N.; Chumlyakov, Y.; Gerstein, G.; Maier, H.J. Giant rubber-like behavior induced by martensite aging in $Ni_{51}Fe_{18}Ga_{27}Co_4$ single crystals. *Scr. Mater.* **2019**, *162*, 387–390. [CrossRef]

20. Chernenko, V.A.; Pons, J.; Cesari, E.; Zasimchuk, I.K. Transformation behaviour and martensite stabilization in the ferromagnetic Co–Ni–Ga Heusler alloy. *Scr. Mater.* **2004**, *50*, 225–229. [CrossRef]

21. Masdeu, F.; Pons, J.; Chumlyakov, Y.; Cesari, E. Two-way shape memory effect in $Ni_{49}Fe_{18}Ga_{27}Co_6$ ferromagnetic shape memory single crystals. *Mater. Sci. Eng. A* **2021**, *805*, 140543. [CrossRef]

22. Masdeu, F.; Pons, J.; Cesari, E.; Kustov, S.; Chumlyakov, Y.I. Magnetic-field-induced strain assisted by tensile stress in $L1_0$ martensite of a Ni–Fe–Ga–Co alloy. *Appl. Phys. Lett.* **2008**, *93*, 152503. [CrossRef]

23. Biswas, A.; Singh, G.; Sarkar, S.K.; Krishnan, M.; Ramamurty, U. Hot deformation behavior of Ni-Fe-Ga-based ferromagnetic shape memory alloy-A study using processing map. *Intermetallics* **2014**, *54*, 69–78. [CrossRef]

24. Pataky, G.J.; Ertekin, E.; Sehitoglu, H. Elastocaloric cooling potential of NiTi, Ni_2FeGa, and CoNiAl. *Acta Mater.* **2015**, *96*, 420–427. [CrossRef]

25. Xiao, F.; Jin, M.; Liu, J.; Jin, X. Elastocaloric effect in $Ni_{50}Fe_{19}Ga_{27}Co_4$ single crystals. *Acta Mater.* **2015**, *96*, 292–300. [CrossRef]

26. Li, Y.; Zhao, D.; Liu, J. Giant and reversible room-temperature elastocaloric effect in a single-crystalline Ni-Fe-Ga magnetic shape memory alloy. *Sci. Rep.* **2016**, *6*, 1–11. [CrossRef]

27. Sarkar, S.K.; Biswas, A.; Babu, P.D.; Kaushik, S.D.; Srivastava, A.; Siruguri, V.; Krishnan, M. Effect of partial substitution of Fe by Mn in $Ni_{55}Fe_{19}Ga_{26}$ on its microstructure and magnetic properties. *J. Alloys Compd.* **2014**, *586*, 515–523. [CrossRef]

28. Barandiarán, J.M.; Chernenko, V.A.; Lázpita, P.; Gutiérrez, J.; Feuchtwanger, J. Effect of martensitic transformation and magnetic field on transport properties of Ni-Mn-Ga and Ni-Fe-Ga Heusler alloys. *Phys. Rev. B* **2009**, *80*, 104404. [CrossRef]

29. Liu, J.; Scheerbaum, N.; Hinz, D.; Gutfleisch, O. Martensitic transformation and magnetic properties in Ni–Fe–Ga–Co magnetic shape memory alloys. *Acta Mater.* **2008**, *56*, 3177–3186. [CrossRef]

30. Sofronie, M.; Tolea, F.; Kuncser, V.; Valeanu, M. Martensitic transformation and accompanying magnetic changes in Ni-Fe-Ga-Co alloys. *J. Appl. Phys.* **2010**, *107*, 1–6. [CrossRef]

31. Nikolaev, V.I.; Yakushev, P.N.; Malygin, G.A.; Averkin, A.I.; Pulnev, S.A.; Zograf, G.P.; Kustov, S.B.; Chumlyakov, Y.I. Influence of partial shape memory deformation on the burst character of its recovery in heated Ni–Fe–Ga–Co alloy crystals. *Tech. Phys. Lett.* **2016**, *42*, 399–402. [CrossRef]

32. Oikawa, K.; Saito, R.; Anzai, K.; Ishikawa, H.; Sutou, Y.; Omori, T.; Yoshikawa, A.; Chernenko, V.A.; Besseghini, S.; Gambardella, A.; et al. Elastic and Superelastic Properties of NiFeCoGa Fibers Grown by Micro-Pulling-Down Method. *Mater. Trans.* **2009**, *50*, 934–937. [CrossRef]

33. Kosogor, A.; L'vov, V.A.; Chernenko, V.A.; Villa, E.; Barandiaran, J.M.; Fukuda, T.; Terai, T.; Kakeshita, T. Hysteretic and anhysteretic tensile stress-strain behavior of Ni-Fe(Co)-Ga single crystal: Experiment and theory. *Acta Mater.* **2014**, *66*, 79–85. [CrossRef]
34. Liu, N.; Huang, W.M. DSC study on temperature memory effect of NiTi shape memory alloy. *Trans. Nonferrous Met. Soc. China (Engl. Ed.)* **2006**, *16*, s37–s41. [CrossRef]
35. Hamilton, R.; Efstathiou, C.; Sehitoglu, H.; Chumlyakov, Y. Thermal and stress-induced martensitic transformations in NiFeGa single crystals under tension and compression. *Scr. Mater.* **2006**, *54*, 465–469. [CrossRef]
36. Panchenko, E.; Timofeeva, E.; Pichkaleva, M.; Tokhmetova, A.; Surikov, N.; Tagiltsev, A.; Chumlyakov, Y. Effect of Stress-Induced Martensite Aging on Martensite Variant Reorientation Strain in NiMnGa Single Crystals. *Shape Mem. Superelasticity* **2020**, *6*, 29–34. [CrossRef]
37. L'vov, V.A.; Rudenko, A.A.; Chernenko, V.A.; Cesari, E.; Pons, J.; Kanomata, T. Stress-induced martensitic transformation and superelasticity of alloys: Experiment and theory. *Mater. Trans.* **2005**, *46*, 790–797. [CrossRef]
38. Karaca, H.E.; Karaman, I.; Lagoudas, D.C.; Maier, H.J.; Chumlyakov, Y.I. Recoverable stress-induced martensitic transformation in a ferromagnetic CoNiAl alloy. *Scr. Mater.* **2003**, *49*, 831–836. [CrossRef]
39. Dadda, J.; Maier, H.J.; Karaman, I.; Karaca, H.E.; Chumlyakov, Y.I. Pseudoelasticity at elevated temperatures in [001] oriented $Co_{49}Ni_{21}Ga_{30}$ single crystals under compression. *Scr. Mater.* **2006**, *55*, 663–666. [CrossRef]
40. Villa, E.; Agilar-Ortiz, C.O.; Álvarez-Alonso, P.; Camarillo, J.P.; Lara-Rodriguez, G.A.; Flores-Zúñiga, H.; Chernenko, V.A. Shape memory behavior of Ni-Fe-Ga and Ni-Mn-Sn ribbons. *MATEC Web Conf.* **2015**, *33*. [CrossRef]
41. Zhao, P.; Dai, L.; Cullen, J.; Wuttig, M. Magnetic and Elastic Properties of $Ni_{49.0}Mn_{23.5}Ga_{27.5}$ Premartensite. *Metall. Mater. Trans. A* **2007**, *38*, 745–751. [CrossRef]
42. Oikawa, K.; Omori, T.; Sutou, Y.; Morito, H.; Kainuma, R.; Ishida, K. Phase Equilibria and Phase Transition of the Ni–Fe–Ga Ferromagnetic Shape Memory Alloy System. *Metall. Mater. Trans. A* **2007**, *38*, 767–776. [CrossRef]